

Structural analysis and transport properties of $(\text{Ru}_{1-x}\text{Co}_x)\text{Sr}_2\text{Gd}_2\text{O}_8$ system

R. Escamilla, A Durán*, and R. Escudero.

Instituto de Investigaciones en Materiales, UNAM, A. Postal 70-360. México D. F.

04510 MÉXICO.

*Centro de ciencias de la Materia Condensada, UNAM, México, D. F. A. Postal 2681,

Ensenada B. C., 22800, MÉXICO.

ABSTRACT

The effects of Co substitution on structural and superconducting properties of $\text{RuSr}_2\text{GdCu}_2\text{O}_8$ compound have been studied. Rietveld refinements of the X-ray diffraction patterns indicate that the cobalt ion progressively replaces ruthenium sites. This replacement induces significant changes on the crystal structure and on the magnetic and superconducting properties. The weak ferromagnetic transition at $T_M = 138.2$ K is shifted at lower temperature, and suppressed at higher Co content. From the crystallographic point of view the Ru-O(1)-Cu bond angle, associated to the rotation of the RuO_6 octahedra, around the c-axis remain essentially constant when Co is substituted by Ru. [This implies that there is not significant Co-induced charge transference to CuO_2 planes]. Furthermore, increasing Co content has the effect to increases the weak ferromagnetic moment, which may be interpreted as the main responsible for breaking the delicate balance between magnetic and superconducting ordering.

Keywords: Ru1212; Rietveld, Crystal structure; ferromagnetism

PACS: 74.62.Bf, 74.62.Dh, 74.72.Bk

1. INTRODUCTION

In $\text{RuSr}_2\text{GdCu}_2\text{O}_8$ (Ru-1212) compound, both ferromagnetic and superconductivity phenomena coexist at the microscopic level [1,2]. The ferromagnetic ordering, appears at a rather high temperature, about 130 – 150 K [3,4], whereas the superconducting transition occurs at low temperature, from about 15 to 45 K. The crystalline structural characteristics of this compound can be described based on the high transition temperature compound: $\text{YBa}_2\text{Cu}_3\text{O}_7$ (Y-123). Ru-1212 contains CuO_2 planes, which are separated by single oxygen-less Gd planes, RuO_2 planes replace the equivalent CuO chains as in the Y-123. In the RuO_2 planes, the Ru atoms is six coordinated, and is forming RuO_6 octahedra. In addition, the structure contains SrO planes

localized between CuO_2 and RuO_2 planes. The O(1) oxygen sites are localized in the SrO planes, whereas the oxygen sites O(2) and O(3) are localized in the CuO_2 and RuO_2 planes, respectively. These planes are connected via the apical oxygen O(1). The role of the CuO_2 planes may be similar to the high T_C cuprates and directly related to the superconducting pairing, whereas RuO_2 planes are related to magnetic order. Several experimental studies have been carried out in order to determine the role of cationic substitutions in RuO_2 sites [5-7, 9]. For instance, studies of heterovalent substitutions in $\text{Ru}_{1-x}\text{M}_x\text{-1212}$ with ($\text{M}=\text{Nb}^{\text{V}+}, \text{Sn}^{\text{IV}+}$) reveal a reduction of magnetism in the RuO_2 planes [8]. Whereas doping Ru sites with $\text{Cu}^{\text{II}+}$, increases the superconducting transition and reduces the magnetic ordering [9]. Actually, the current understanding of the physical characteristics of this system is that superconductivity and ferromagnetic ordering are originated in the CuO_2 and RuO_2 planes, respectively. However, the nature of the competition/coexistence of both phenomena so far, requires further understanding. In this context we are reporting studies on the effect of cobalt substitution in Ru sites. The study emphasizes on the changes in the crystalline structure and effects on the superconducting and magnetic properties.

2. EXPERIMENTAL

Polycrystalline samples of $(\text{Ru}_{1-x}\text{Co}_x)\text{Sr}_2\text{GdCu}_2\text{O}_8$ ($x = 0, 0.025, 0.05, 0.075, 0.1, 0.2$) were synthesized by solid state reaction of oxides: RuO_2 (99%), CoO (99.999%), Gd_2O_3 (99.9%), CuO (99.99%) and SrCO_3 (98+%). After calcinations in air at 900°C , the samples were grounded, pressed into pellets and annealed in oxygen at 1000°C . Phase identification was performed using a X-ray diffractometer, Siemens D5000 with Cu-K_α radiation and Ni filter. Intensities were measured in steps of 0.02 degrees for 14 seconds in the 2θ range from 5 to 120, at room temperature. Crystallographic phases were identified by comparison with X-ray patterns in the JCPDS database. The crystalline structure was refined with the program Quanto [10] (Rietveld program for quantitative phase analysis of polycrystalline mixtures with multi-phase capability). The Bond Valence Sum program was used to distinguish the oxidation states of metals Ru and Cu [11]. The superconducting transition temperatures were determined with a closed-cycle helium refrigerator by measuring the resistance vs. temperature characteristic by the standard four-probe technique, from 250 K to 14 K. Measurements of ac susceptibility, dc susceptibility, and magnetization versus magnetic field were carried out using a superconducting Quantum Interference Device Magnetometer, (MPMS Quantum Design), from 2 to 300 K and applied field up to ± 40 kOe.

3. RESULTS AND DISCUSSION

Figure 1 shows X-ray diffraction patterns for the $\text{Ru}_{1-x}\text{Co}_x\text{-1212}$ samples. The structural analysis indicate that all samples correspond to the Ru-1212 structure, with negligible content of $\text{Sr}_3(\text{Ru,Cu})\text{O}_7$ (ICDD n° 51-0307), SrRuO_3 (ICDD n° 28-1250), and for $x \geq 0.1$ display slight traces of $\text{RuSr}_2\text{Gd}_2\text{Cu}_2\text{O}_{10}$. In the process of refinement we took into account the presence of secondary phases and the substitution of Co ions in Ru and Cu sites. Fig. 2 shows an example; a fitted patterns for the undoped sample. Detailed results of the structural refinements are listed in Table 1, the first three rows show the trend of change of the lattice parameters at room temperature with increase cobalt content. It is observed that as x is increased, the c -axis parameter decreases, mainly as a result of the decrease of the Ru/Co-O(1) average bond length. The a -axis increases slightly, and as consequence of those changes the unit-cell volume decreases slightly. This result may be explained considering the co-ordination numbers and the ionic radii of the $\text{Co}^{\text{III}+}$, $\text{Cu}^{\text{II}+}$ and $\text{Ru}^{\text{V}+}$ ions. It is noted that the $\text{Co}^{\text{III}+}$ radius with six co-ordination number changes from 0.545 to 0.61 Å for low spin and high spin configuration, respectively. Whereas $\text{Cu}^{\text{II}+}$ with a size of 0.65 Å in five co-ordination number, and $\text{Ru}^{\text{V}+}$ in six co-ordination number has a size of 0.565 Å [12]. From these values, it is clear that the decrease of the unit cell volume can be related to the substitution of $\text{Co}^{\text{III}+}$ in low spin configuration state into the $\text{Ru}^{\text{V}+}$ sites. This behaviour is consistent with the observed changes in $\text{Y}_1\text{Ba}_2\text{Cu}_3\text{O}_7$, when $\text{Co}^{\text{III}+}$ is substituted in low spin configuration into the CuO chains [13].

From results of our structural refinement, we can conclude that cobalt atoms majority occupy the Ru sites, which give place to significative changes on the Ru/Co–O(1) bond length, rather than in the Ru/Co – O(3) bond length. As a consequence, an increase in the octahedral distortion (Δ_{oct}) is observed; from 0.184 Å ($x = 0.0$) to 0.287 Å ($x = 0.2$), see Table 2. Furthermore, the Ru – O(1) – Cu bond angle associated to the rotation of RuO_6 octahedra around the c -axis, remains essentially constant. In contrast, the Cu–O(2)–Cu buckling angle changes from 169.2° ($x = 0.0$) to 167.99° ($x = 0.2$). On the other hand, from Bond Valences the pentavalent state of Ru ion is confirmed, however this result is inconsistent with previous results obtained by NMR and XANES studies indicating mixed ionic states with 40% $\text{Ru}^{\text{IV}+}$ and 60% $\text{Ru}^{\text{V}+}$ [14, 15]. The Bond Valences analysis suggests that the charge transfer between RuO_2 and CuO_2 planes does not change. Consequently, the magnetic and transport properties are not driven by structural induced changes in the conduction band as have been proposed by others authors [6, 16]. Regardless of this fact, the continuous introduction of Co ions into RuO_2 planes give rise to notable changes on the magnetic and superconducting

transitions as already have been noted. Temperature dependence of normalized resistance at zero external field for all samples is shown in Fig. 3. For the sample with $x = 0$, the resistance shows a metallic-like behaviour with a superconductivity onset at about 57 K, and reaching zero resistance at 33 K. Contrarily, doped samples do not display superconductivity below 10 K. For composition with $x=0.025$, the normal state resistance starts to increase at high temperature with a downturn at low temperature, while for higher compositions $x > 0.025$ a semiconducting-like behaviour is observed. In the inset of Fig. 3 we show the real part of the ac susceptibility data, for the undoped sample. A small upward at about 138.2 K marks the onset of the spontaneous magnetisation, indicating the weak ferromagnetic transitions (T_M). At 35 K it is noted a continuous decreasing of the ac susceptibility indicating the superconducting transition, but without diamagnetic signal. This fact might indicate either microstructural effects connected with sample granularity (macroscopic screening currents) [17] or competing effects between magnetism and superconducting ordering as have been observed in rare earth intermetallic compounds [18]. These ac data show that our samples are structurally comparable to other samples produced and reported in other laboratories [3, 4].

We performed measurements of dc susceptibility as function of temperature at low magnetic field (15 Oe), in zero field cooling (ZFC) from 300 K to 2 K, as is shown in Fig. 4, Meissner effect is not observed. The inset of Fig. 4 shows the effect of Co substitution on the magnetic characteristics for all samples. The ferromagnetic T_M and the antiferromagnetic T_N transitions are clearly seen with help of the susceptibility derivative data (dy/dT). The results reveal that T_M decreases as Co is increased, and disappears at a concentration of $x = 0.20$. Moreover, in the range of compositions for $x < 0.1$ we observed a clear splitting of the ZFC and FC measurements, close to T_M which disappears for sample with $x = 0.2$ (in the inset we are presenting only the ZFC measurement). It is important to note that not only the Co concentration has effect on T_M , but also the external magnetic field, as is illustrated in Fig. 5 a). There, it seems that as the Co concentration is increased the magnetic transition T_M is shifted to low temperatures, depending on the applied field. Furthermore, increasing the magnetic field, shifts T_M to high temperature for depending on Co concentration; for example, at 1 kOe T_M is about 133 K when $x = 0.025$, but when the field is 30 kOe, T_M is shifted to about 155 K. T_M disappears for the composition with $x = 0.1$ when the field is 30 kOe. Thus, both the Co concentration and the magnetic field may destroy T_M . On the other hand, in Fig. 5 b) we show that T_N is affected notably only by the intensity of the magnetic field, Co concentration has no effect. In this figure is observed that T_N is shifted from 8 K at 1 kOe to about 2.6 K at 30 kOe. This behaviour is quite

typical of layered structures; the external magnetic field tends to saturate the paramagnetic moment of the Gd sublattice [19]. Thus, susceptibility results suggest that the dominant magnetic character is antiferromagnetic order (AFM) at low temperatures, and canted ferromagnetism at high temperature since the transverse components of spins differ from one crystallographic site to another and the equilibrium angles depend on both the external magnetic field and dopant content. These experimental evidences have been well documented in doped manganites, cuprates and intermetallic compounds [19-21]. In Fig 6 we plotted the inverse molar susceptibility ($1/\chi$) as a function of Co concentration measured at 1 kOe from 170 to 300 K. Here we used a fit to the Curie-Weiss (C-W) law $\chi = C/(T-\Theta)$ considering the superposition of Gd and Ru sublattices as independent contribution to C-W. The theoretical values for isolated Gd^{+3} ion was kept constant at $\mu_{eff} = 7.94 \mu_B$ and $\Theta = -4K$. The Ru contributions (μ_{eff} , Θ_{Ru}) were estimated for each concentration and are plotted in the inset of Fig. 6. A continuous increase of the effective moments is seen from $\sim 1.06 \mu_{eff}$ for $x = 0$ to $2.60 \mu_{eff}$ for $x = 0.10$, after that with further Co increase the effective moment is reduced to $\sim 0.91 \mu_{eff}$. On the other hand, the Curie temperature, Θ_{Ru} changes from 153.9 ± 0.5 to 112 ± 2.5 degrees, for $0.025 < x < 0.10$ and then increase again from $x > 0.10$ to a value about 157.7 ± 1.2 degrees. To have a better understanding of this magnetic behaviour, we performed magnetisation versus applied magnetic field (M-H) measurements at $T = 2 K$ (see Fig 7). The hysteresis loops at low field (main panel) is attributed to the weak magnetism of the Ru/Co sublattice, whereas the dependence of the magnetization at high field region (inset B) to the antiferromagnetic order of Gd ion. A trend to saturation is observed with value at about $7.8 \mu_B/f.u.$, which correspond to the Gd moment, as obtained by neutron diffraction studies ($\sim 7.0 \mu_B$) [22]. This experimental value confirms the two expected contributions: The Gd moment, plus $0.8 \mu_B/f.u.$ due to Ru+5 sublattice at low spin state ($1\mu_B$ for $3d^3$, $S=1/2$). On the other hand, the behaviour of the remanent magnetization (M_R) associated to the Ru sublattice as dependence of Co content is plotted in inset A). M_R is increased from $0.14 \mu_B/f.u.$ for $x = 0$ to $0.49 \mu_B/f.u.$ for $x = 0.05$ and then decreases to $0.05 \mu_B/f.u.$ at a concentration about $x = 0.2$. The small value of M_R for $x = 0$ is consistent with the analysis of neutron diffraction measurements by Lynn et al [22], where an upper limit of about $0.1 \mu_B$ was obtained for the ferromagnetic peaks below of T_M . Again, it is worthwhile to note that M_R as well as μ_{eff} extracted from Ru

sublattice (inset of Fig. 6) are increased as Co is introduced in the Ru sublattice (for $x < 0.1$). This behaviour is opposed to Sn and Nb as in Eu-1212 [16]. However, these characteristics are still more intriguing in the Ce, Eu-1222 [23] and Gd-1212 [24] compounds doped with iron where a decreasing of the magnetic moment in the Ru sublattice was observed. It is possibly that this increasing of the magnetic moment in the Ru/Co site may be due to an enhancement of the antisymmetric exchange, causing the effect that spins be canted in the ab-plane as it has been argued in several intermetallic and ruthenocuprate compounds [19, 21, 25, 26], where a delicate balance among the subtle variation in composition, magnetic structure, and superconducting state may exist. Furthermore, recent studies [27] have shown that complete substitution; Ru by Co, gives a paramagnetic material which is accomplished by depleting oxygen in the structure. The drastic reduction of magnetic moment for $x > 0.1$ accompanied with the strong octahedral distortion observed here could be related to this fact.

4. CONCLUSIONS

In summary, we have presented a detailed crystallographic and magnetic study of the $(\text{Ru}_{1-x}\text{Co}_x)\text{Sr}_2\text{GdCu}_2\text{O}_8$ system by x-ray diffraction at room temperature and magnetisation measurements. X-ray diffraction results indicate that Co ions occupy the Ru sites. This replacement causes significant changes in the Ru - O(1) bond length inducing an increase in the octahedral distortion. Contrarily to previous report, we found that the bond angle associated to the rotation around the c-axis remain essentially constant, beside, our results from bond valence summations do not show changes in the average valence of Ru/Co and Cu ion, so that no evidence of Co-induced charge transference between RuO_2 and CuO_2 planes exist. Finally, we found from magnetic measurements that a gradual introduction of Co-ions into the structure, enhance the magnetic moment, μ_{eff} and M_R via the ferromagnetic component. Thus we believe that this increase of the magnetic moment might be responsible for the delicate balance between weak ferromagnetism and superconductivity via pair breaking or trapping holes in the CuO_2 planes.

Acknowledgments

Economical support is acknowledged to UC-MEXUS, and DGAPA-UNAM. M. Sainz and F. Silvar for technical support and D. Bucio for assistance in sample preparation

REFERENCES

- [1] J.L. Tallon, C. Bernhard, M.E. Bowden, P.W. Gilberd, T.M. Stoto, and D. Pringle, *IEEE Trans. Appl. Supercond.* **9**, (1999) 1696.
- [2] C. Bernhard, J.L. Tallon, Ch. Niedermayer, Th. Blasius, A. Golnik, E. Brücher, R. Kremer, D. Noakes, C. Stronach, E. Ansaldo, *Phy. Rev. B* **59** (1999) 14099.
- [3] I Felner, U. Asaf, S. Reich, and Y. Tsabba, *Physica C* **311** (1999) 163
- [4] P.W. Klamut, B. Dabrowski, M. Maxwell, J. Mais, O. Chmaissem, R. Kruk, R. Kmicc, and C. W. Kimball, *Physica C* **341-348** (2000) 455
- [5] J.L. Tallon, *IEEE Trans. Appl. Supercond.* **9** (1999) 1696.
- [6] A.C. McLaughlin, and J.P. Attfield, *Phys. Rev. B* **60** (1999) 14605.
- [7] P. W. Klamut, B. Dabrowski, J. Mais and M. Maxwell, *Physica C* **350** (2001) 24.
- [8] A.C. McLaughlin, V. Janowitz, J.A. McAllister, J.P. Attfield, *Chem. Commun.* **14**, (2000) 1331
- [9] P.B. Klamut, B. Dabrowski, S. Kolesnik, M. Maxwell, and J. Mais., *Phys. Rev. B* **63** (2001) 224512
- [10] Altomare, A., Burla, M.C., Giacovazzo, C., Guagliardi, A., Moliterni, A.G.G., Polidori, G., Rizzi, R. *J.Appl. Cryst.* **34** (2001) 392
- [11] A. S. Wills and I.D. Brown, *Valist*, CEA, France (1999). Program available from <ftp://ftp.ill.fr/pub/dif/valist/>
- [12] R. D. Shannon. *Acta Crystallogr.* **A32**, 751 (1976).
- [13] Miceli P F, Tarascon J M, Greene L H, Barboux P, Rotella F J and Jorgensen J D 1988 *Phys. Rev. B* **37** 59
- [14] Ken-ichi Kumagai, Satomi Takada, and Yuji Furukawa, *Phys. Rev. B* **63** (2001) 180509.
- [15] R. S. Liu, L.-Y. Jang, H.-H. Hung, and J. L. Tallon *Phys. Rev. B* **63** (2001) 21250.
- [16] G.V.M. Williams, H.K. Lee and S. Krämer, *Phys. Rev. B* **67** (2003) 104514
- [17] A. C. McLaughlin, W. Zhou, and J. P. Attfield, A. N. Fitch and J. L. Tallon, *Phys. Rev. B* **60** (1999) 7512
- [18] A. Durán, E Muñoz, S. Bernès and R. Escudero, *J. Phys.: Condens. Matter* **12** (2000) 7595.
- [19] B. K. Cho, P. C. Canfield and D. C. Johnston, *Phys. Rev. B* **53** (1996) 8499
- [20] I. G. Deac, J. F. Mitchell, P. Schiffer, *Phys. Rev. B* **63** (2001) 172408,
- [21] H. D. Coffey, T. M. Rice, F. C. Zhang, *Phys. Rev. B* **44** (1991) 10112.

- [22] J. W. Lynn, B. Keimer, C. Ulrich, C. Bernhard, and J. L. Tallon, *Phys. Rev. B* **61**, (2000) R14 964.
- [23] I. Felner, U. Asaf, *Physica C* **292** (1997) 97
- [24] R. Escamilla, F. Morales, T. Akachi and R. Gómez. Submitted to Supercond. Sci. Technol
- [25] J. W. Lynn, S. Skanthakumar, Q. Huang, S. K. Sinha, Z. Hossain, L. C. Gupta, R. Nagarajan, C. Godart, *Phys. Rev. B* **55** (1997) 6584
- [26] A. Duran, S. Bernes, R. Escudero, *Phys. Rev. B* **66** (2002) 212510.
- [27] W. P. S. Awana, S. K. Malik, W. B. Yelon, M. Karppinen, H. Yamauchi, *Physica C* **378-381** (2002) 155.

FIGURE CAPTION

Fig. 1 X - ray diffraction patterns for the $\text{Ru}_{1-x}\text{Co}_x$ -1212 samples. The symbols +, * and o represent impurities of SrRuO_3 , $\text{Sr}_3(\text{Ru,Cu})\text{O}_7$ and Ru:1222, respectively.

Fig. 2 Rietveld refinement on the X-ray diffraction pattern for the $x = 0.0$ sample. Experimental spectrum (dots), calculated pattern (continuous line), difference (middle line) and the calculated peaks positions (bottom).

Fig. 3 Normalized resistances as a function of temperature in $(\text{Ru}_{1-x}\text{Co}_x)$ -1212 for different Co concentrations as indicated in the figure. Inset shows ac susceptibility for $x = 0.0$ measured at 730 Hz and field amplitude of 3.0 Oe.

Fig. 4 dc susceptibility measurements as a function of temperature for $(\text{Ru}_{1-x}\text{Co}_x)$ -1212 . We show the ZFC mode with an external magnetic field of 15 Oe. The inset shows $d\chi/dT$ vs T for $0 < x < 0.2$ composition.

Fig. 5 a) Behavior of T_M as a function of Co content at several applied magnetic fields b)
Antiferromagnetic transition T_N as a function of applied magnetic field. T_N is independent of Co content.

Fig. 6. Temperature-dependent of the inverse molar susceptibility $1/\chi$ for $(\text{Ru}_{1-x}\text{Co}_x)$ -1212 with $0.025 < x < 0.2$ at 1 kOe. Inset shows the effective moments μ_{eff} and the Curie-Weiss temperature for Ru sublattice as a function of Co content (the line is guided to the eye).

Fig. 7. Hysteresis loops in the low field region for $(\text{Ru}_{1-x}\text{Co}_x)$ -1212 with $x = 0$ (full square), 0.05 (open triangles), 0.1 (full triangles) and 0.2 (solid line). Inset a) shows the remanent moment (M_R) as a function of Co content (the solid line is guided to the eye). Inset b) shows magnetisation at high field 40 kOe for $x = 0$ (full square), $x = 0.075$ (open circle) and $x = 0.2$ (solid line).

TABLE CAPTION

Table 1 Structural Parameters for $\text{Ru}_{1-x}\text{Co}_x$ -1212 at 295 K.

Table 2 Bond lengths (\AA), bond angles (deg) and octahedral distortion (Δ_{oct}) for $\text{Ru}_{1-x}\text{Co}_x$ -1212.

Figure1

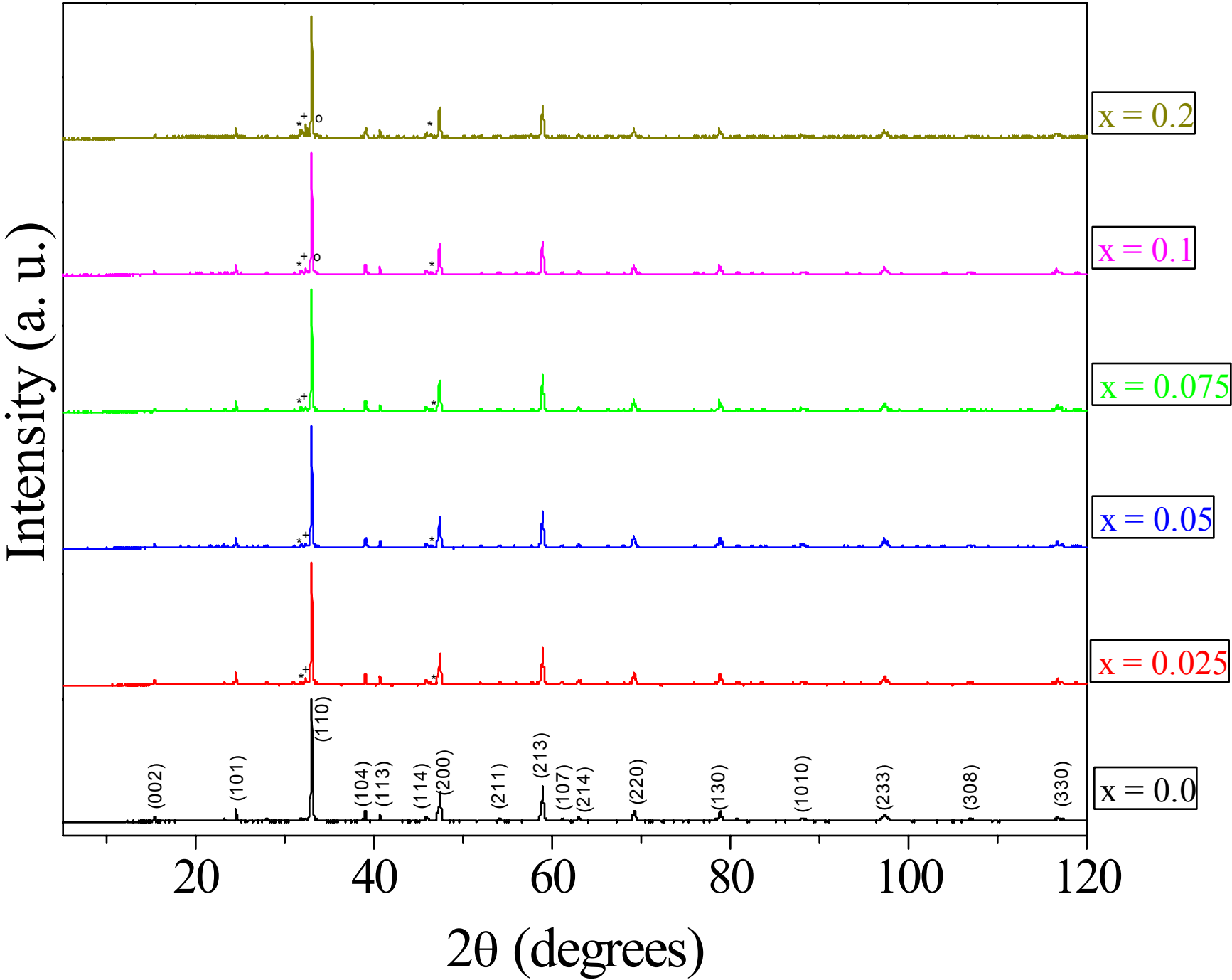


Figure2

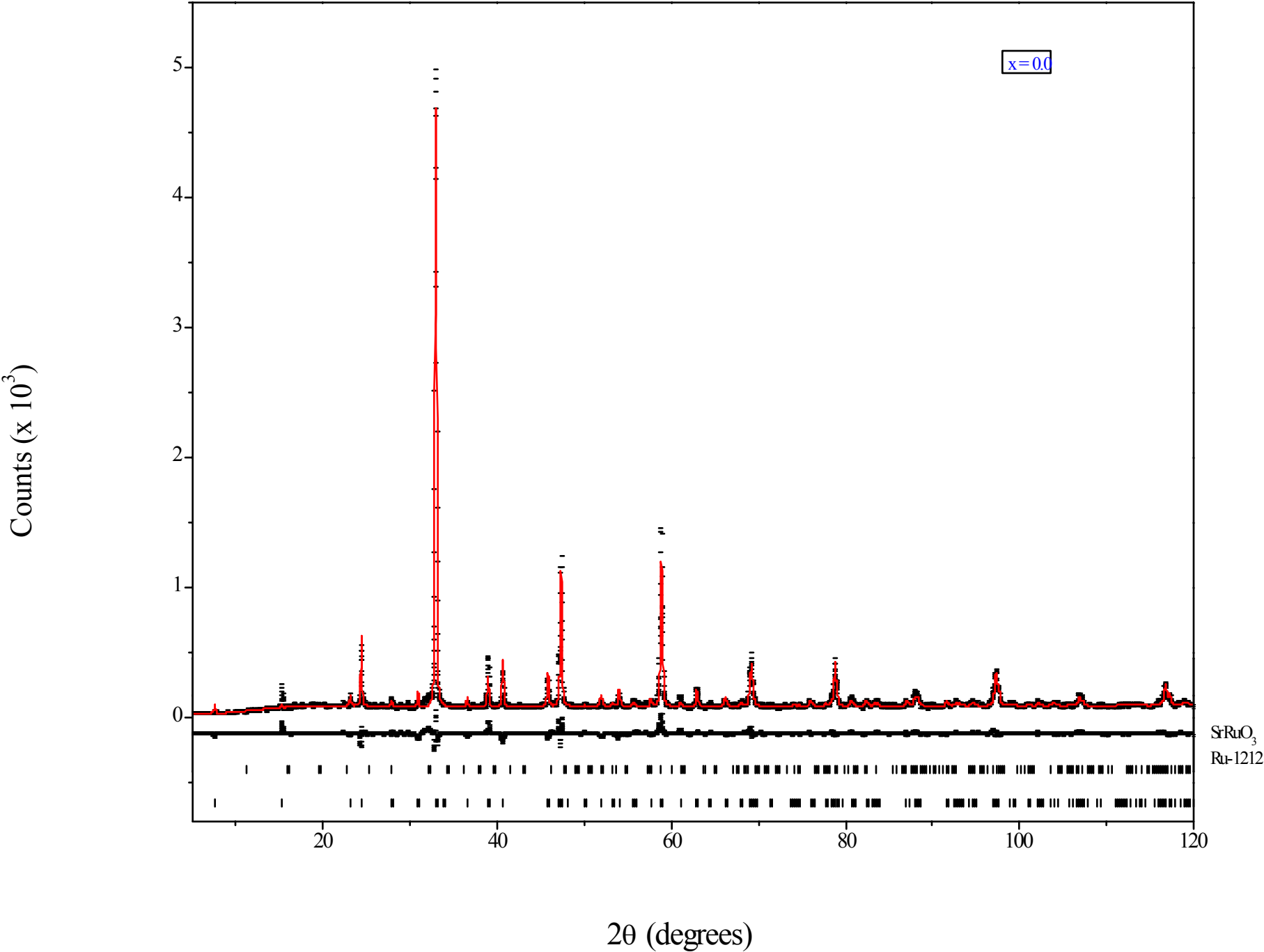


Figure3

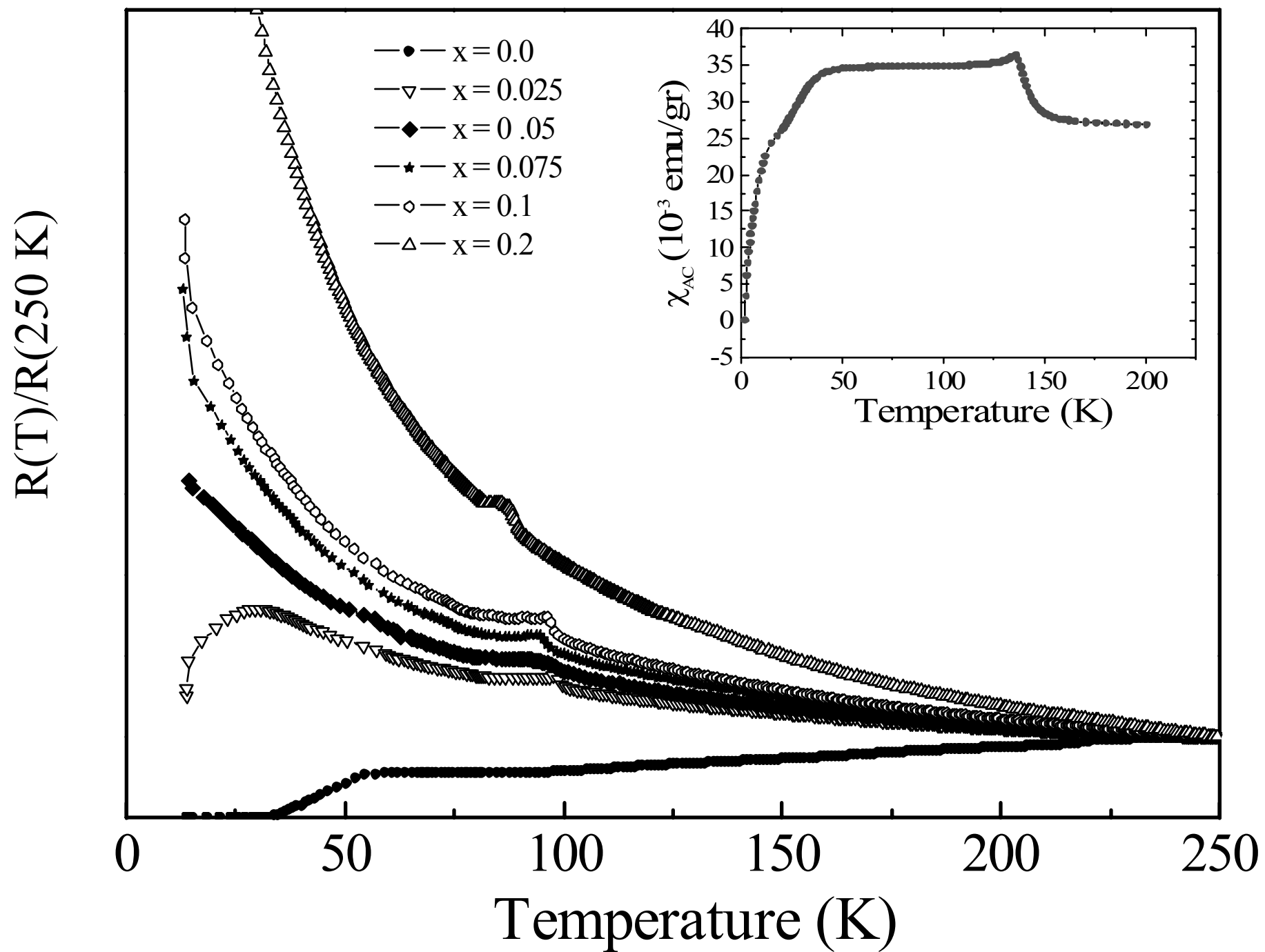
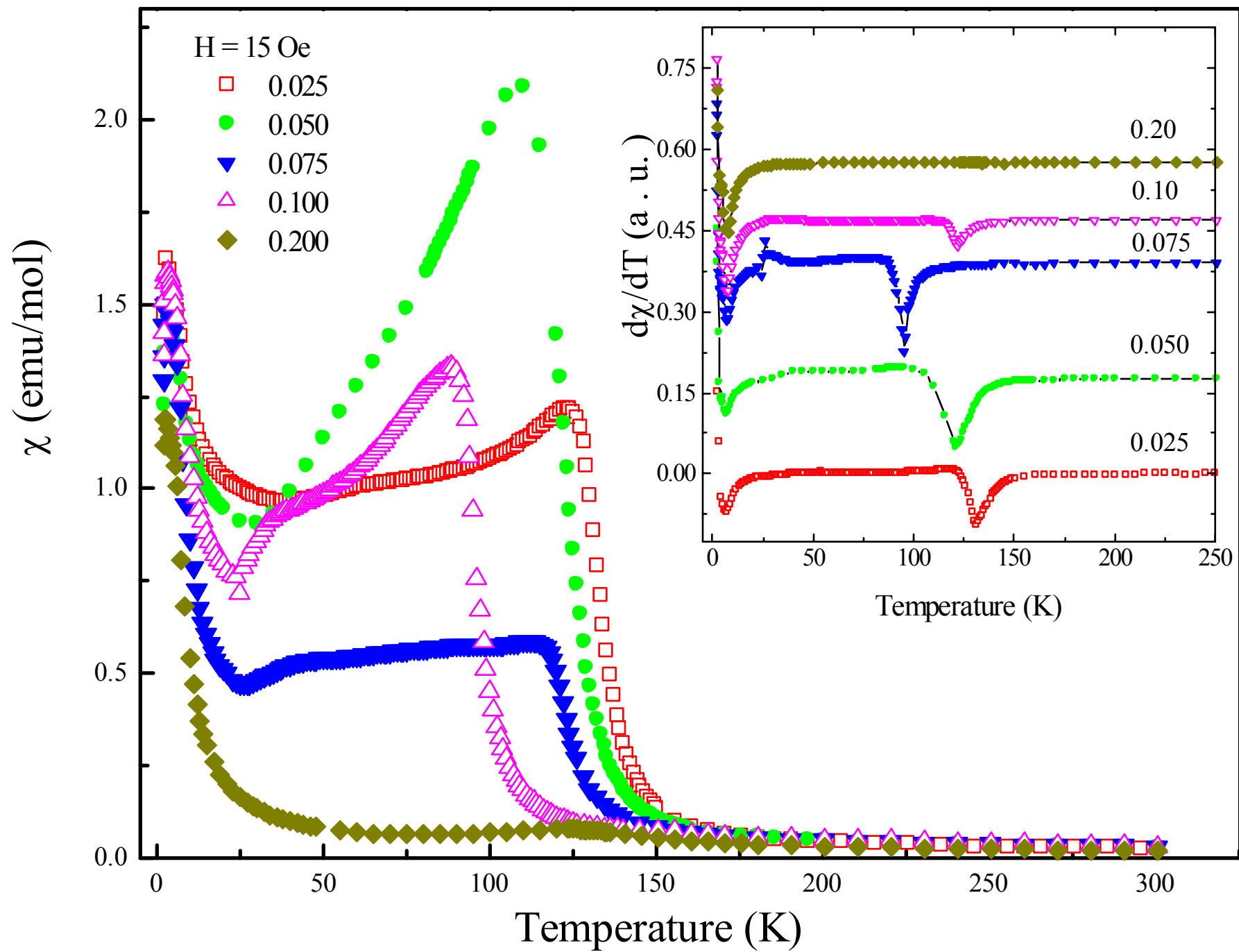


Figure4



Co Concentration (x)

0.025

0.050

0.075

0.100

T_m (K)

a)

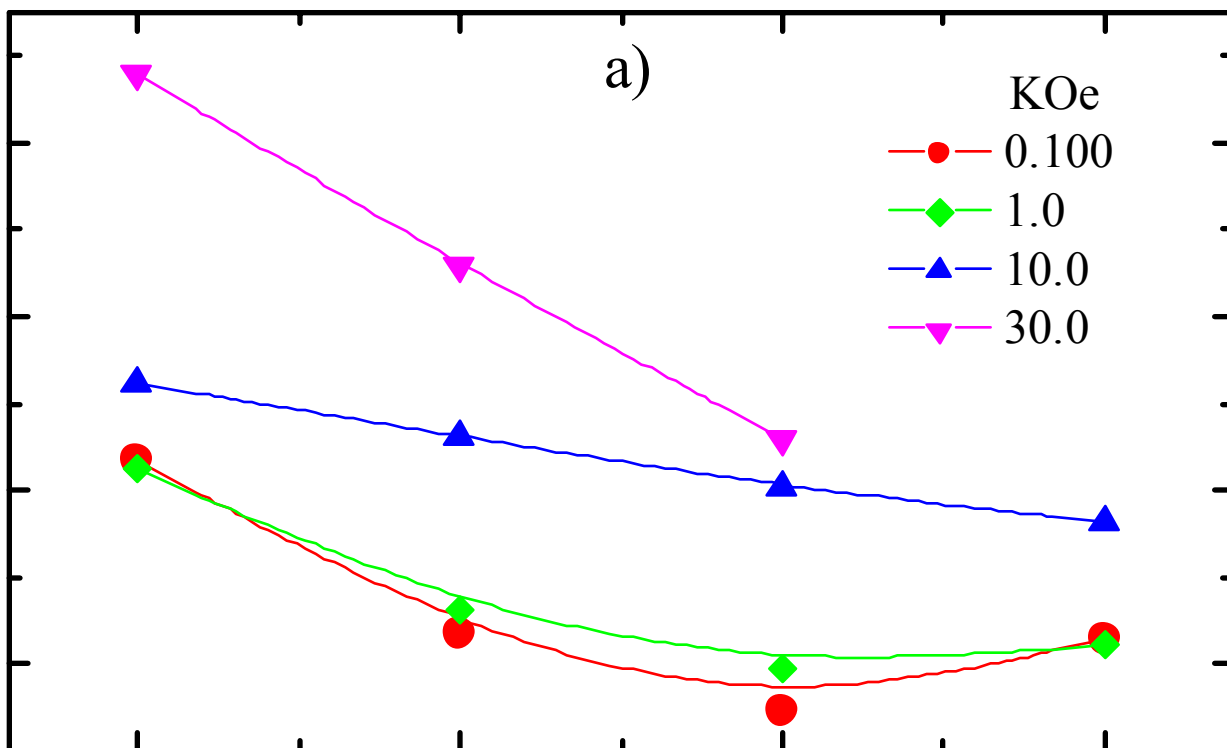
KOe

0.100

1.0

10.0

30.0



b)

T_N (K)

8

7

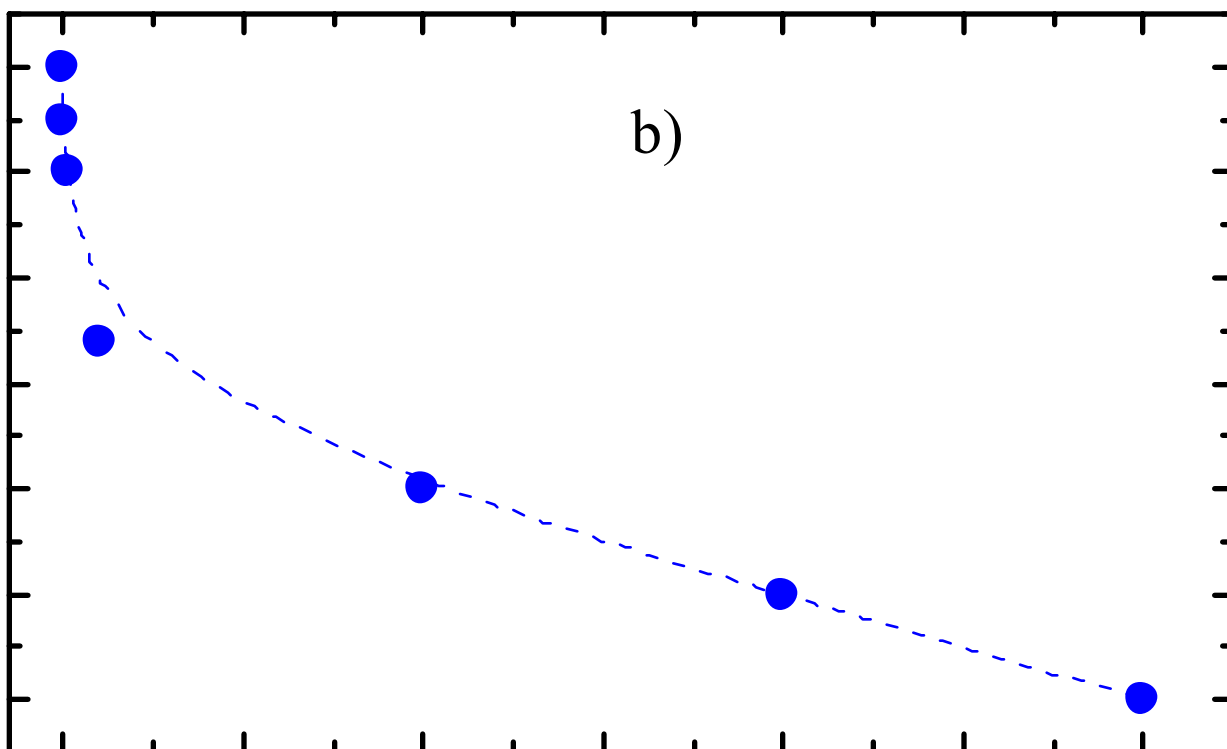
6

5

4

3

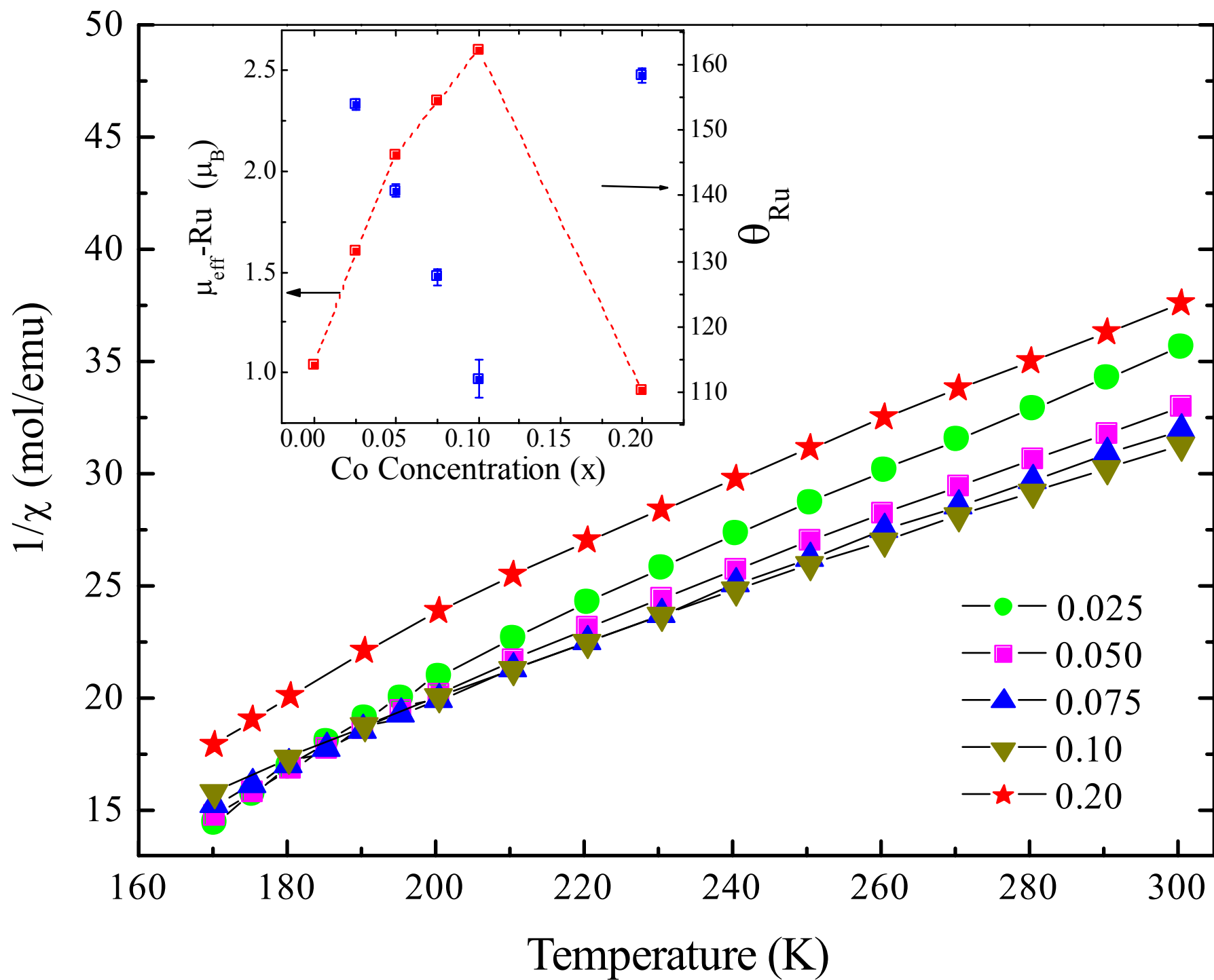
2



Applied Magnetic Field (kOe)

Figure5

Figure6



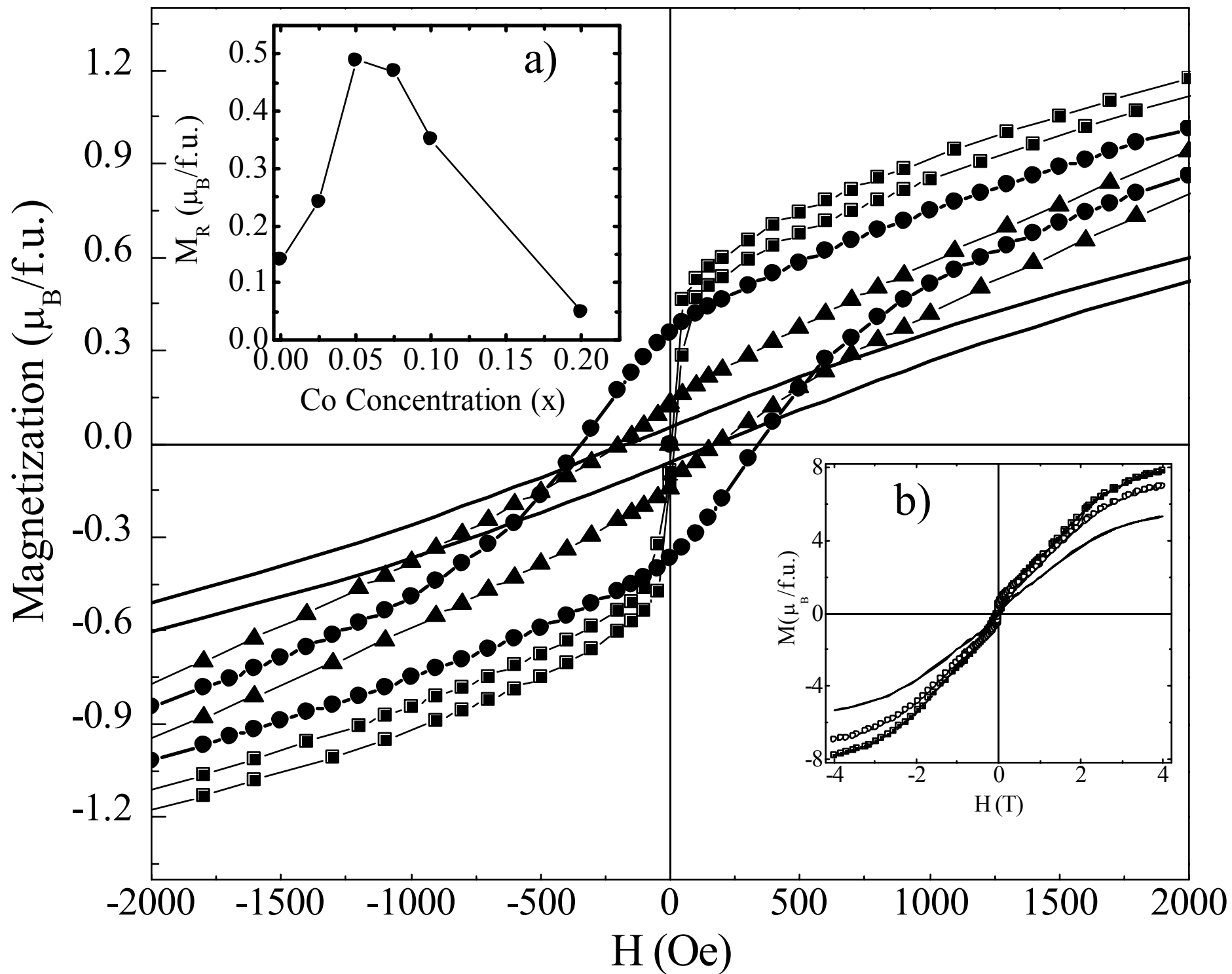


Figure7

TABLE 1

(x=)		0.0	0.025	0.05	0.075	0.1	0.2
	a(Å)	3.8367(3)	3.8374(2)	3.8382(2)	3.8388(4)	3.8393(4)	3.8408(4)
	c(Å)	11.568(3)	11.5622(2)	11.5584(3)	11.5544(3)	11.5505(4)	11.5417(4)
	V(Å ³)	170.29	170.26	170.28	170.27	170.25	170.25
Ru/Co	S _{ij} (v.u.)	4.98	4.99	4.97	4.98	5.04	4.97
	B(Å ²)	0.82(9)	0.86(8)	1.39(8)	0.82(8)	0.74(8)	1.5(1)
	N	-	0.02(1)	0.04(2)	0.07(2)	0.09(1)	0.18(1)
Gd	B(Å ²)	2.06(7)	1.72(6)	1.52(6)	2.09(6)	1.53(5)	2.09(9)
Sr	z	0.3067(4)	0.3067(4)	0.3066(2)	0.3066(2)	0.3066(2)	0.3066(2)
	B(Å ²)	0.84(7)	0.50(5)	0.99(7)	0.70(5)	0.54(5)	0.25(7)
Cu	z	0.1452(2)	0.1455(2)	0.1456(3)	0.1457(3)	0.1457(3)	0.1470(3)
	S _{ij} (v.u.)	2.11	2.11	2.11	2.11	2.10	2.08
	B(Å ²)	1.04(8)	1.40(7)	0.70(8)	0.43(23)	0.98(6)	1.2(1)
O(1)	x	0.0390	0.0390	0.0390	0.0390	0.0390	0.0390
	z	0.3335(3)	0.3337(3)	0.3338(4)	0.3339(4)	0.3347(4)	0.3347(4)
	B(Å ²)	5.8(8)	5.4(7)	3.9(6)	7.2(7)	6.9(7)	8.5(1.3)
O(2)	z	0.1295(1)	0.1297(4)	0.1295(3)	0.1295(3)	0.1295(4)	0.1295(4)
	B(Å ²)	2.9(4)	2.1(3)	0.7(2)	1.0(3)	2.0(3)	1.9(5)
O(3)	x	0.1140	0.1140	0.1140	0.1140	0.1140	0.1140
	B(Å ²)	5.8(6)	5.8(5)	5.7(4)	5.6(4)	5.1(5)	5.1(8)
%Gd1212		94.91(2)	95.83(1)	95.43(1)	93.28(2)	86.16(3)	83.40(6)
%SrRuO ₃		2.1(1)	3.8(1)	2.70(8)	5.1(1)	3.1(1)	8.0(1)
%Sr ₃ Ru ₂ O ₇		2.9(4)	0.3(2)	1.9(2)	1.6(3)	3.3(3)	6.7(8)
%Gd1222						1.2(1)	1.8(1)
	R _p (%)	8.8	6.0	5.9	6.0	5.9	6.5
	R _{wp} (%)	11.5	8.3	8.2	8.7	8.0	9.1
	R _{exp} (%)	9.2	3.7	3.6	3.6	3.6	3.7
	χ ² (%)	1.2	2.2	2.3	2.4	2.2	2.5

Note. Space group: *P4/mmm* (# 123). S_{ij} (v.u.) is the Bond Valences, N is the cobalt occupancy factor, Atomic positions: Ru: 1b (0, 0, ½); Gd: 1c (½, ½, 0); Sr: 2h (½, ½, z); Cu: 2g (0, 0, z); 2O(1) in 8s (x, 0, z) × 1/4, 4 O(2) in 4i (0, ½, z), and 2O(3) in 4o (x, ½, ½) × 1/2 position.

^a % of impurity in the phase

TABLE 2

x =	0.0	0.025	0.05	0.075	0.1	0.2
Ru- O(1): 2	1.931	1.931	1.928	1.926	1.924	1.914
Ru – O(3): 4	1.967	1.968	1.968	1.969	1.969	1.970
$\langle \text{Ru} - \text{O} \rangle_{\text{average}}$	1,956	1,956	1,955	1,955	1,954	1,951
Δ_{oct}	0,184	0,189	0,205	0,220	0,230	0,287
Cu - O(1)	2.182	2.182	2.180	2.180	2.179	2.171
Cu - O(2)	1.927	1.927	1.928	1.928	1.929	1.931
Ru-O(3)-Ru	154.32	154.31	154.31	154.31	154.31	154.31
Cu-O(2)-Cu	169.22	169.1	168.92	168.86	167.98	167.99
Ru-O(1)-Cu	171.62	171.62	171.61	171.60	171.57	171.55